ChemComm

Effects of Surface Acidity on the Structure of Organometallics Supported on Oxide Surfaces

Journal:	*ChemComm*
Manuscript ID	CC-FEA-01-2023-000047.R2
Article Type:	Feature Article

SCHOLARONE™
Manuscripts

ARTICLE

Effects of Surface Acidity on the Structure of Organometallics Supported on Oxide Surfaces

Kavyasripriya Samudrala and Matthew P. Conley*

Well-defined organometallics supported on high surface area oxides are promising heterogeneous catalysts. An important design factor in these materials is how the metal interacts with the functionalities on an oxide support, commonly anionic X-type ligands derived from the reaction of an organometallic M–R with an –OH site on the oxide. The metal can either form a covalent M–O bond or form an electrostatic $M^+\cdots{}^-O$ ion-pair, which impacts how well-defined organometallics will interact with substrates in catalytic reactions. A less common reaction pathway involves the reaction of a Lewis site on the oxide with the organometallic, resulting in abstraction to form an ion-pair, which is relevant to industrial olefin polymerization catalysts. This Feature Article views the spectrum of reactivity between an organometallic and an oxide through the prism of Brønsted and/or Lewis acidity of surface sites and draws analogies to the molecular frame where Lewis and Brønsted acids are known to form reactive ion-pairs. Applications of the well-defined sites developed in this article area also discussed.

Introduction

Brønsted and Lewis acidity are two of the most deeply ingrained concepts in all of chemistry. For example, manipulation of Brønsted acid strength using acid dissociation constants (i.e. pK_a) is part of the general chemistry curriculum and is one of the clearest examples of a structure property relationship. We suspect that nearly all the readers of this article would be able to rank acid strength in the order $HCl < H_2SO_4 < HSO_3CF_3$.
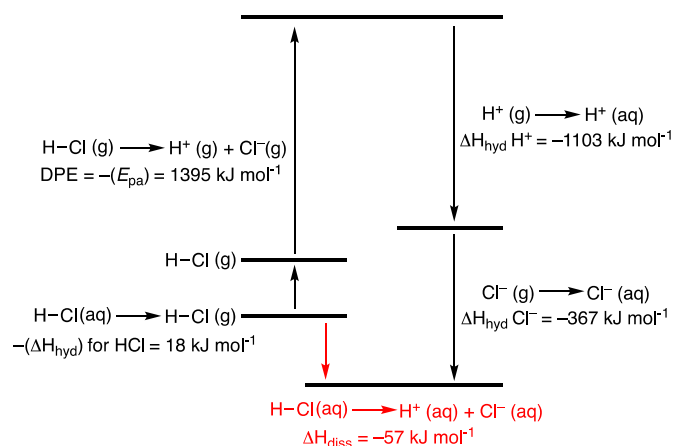

Figure 1. Haber-Born cycle giving the energetics for HCl dissolution in water. Values in the figure and cited in the text are taken from ref 2 and 3. ΔH_{hyd} is taken from ref 4.

Common pK_a or Hammett acidity scales for liquid acids include significant solvation energies that ultimately drive acid dissociation in solution. The Haber-Born cycle shown in Figure 1 for aqueous HCl illustrates this point. Heterolytic cleavage of HCl to form H^+ and Cl^- is endothermic, which is characteristic of all HX acids, and is usually measured as the deprotonation energy (DPE = $-E_{pa}$; E_{pa} = proton affinity). The driving force for HCl dissociation in aqueous media is entirely driven by ΔH_{hyd} for H^+ and Cl^-. This also explains why acidity trends often change when moving from water to polar aprotic MeCN. HCl acts as a weaker acid in MeCN (pK_a(MeCN) = 10.4) than it does in H_2O ($pK_a(H_2O)$ = –8);[1] ΔH_{diss} decreases to –34.7 kJ mol⁻¹ driven mostly by the decrease in ΔH_{MeCN} for Cl^- (347.7 kJ mol⁻¹, ΔH_{MeCN} for H^+ = –1100 kJ mol⁻¹).[2-4]

Measuring the Brønsted strength of solid acids is challenging. For example, acidic oxides react with bases (e.g. pyridine, NH_3, PR_3, etc.) to form ion-pairs, Figure 2.[5-7] Experimentally, adsorption/desorption techniques give ΔH_{abs}, but these values do not typically scale with acid strength as expected for Hammett acids.[8, 9] Indeed, the thermodynamic cycle shown in Figure 2 shows that DPE and E_{pa} of the base are included in ΔH_{abs}, but a third $\Delta H_{ion-pair}$ is also necessary in a 1:1 adduct. In essence, the solvation terms driving the dissociation of HX in solution are absent on an oxide surface.
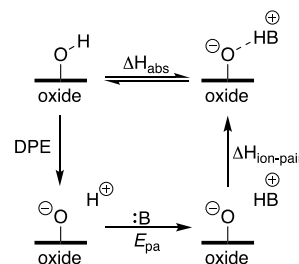
a. Department of Chemistry, University of California, Riverside, California 92521, United States

Figure 2. Thermodynamic steps involved in the adsorption of a base onto an acidic support.

This challenge is not unique to oxides. Solid carborane acids are the strongest known Brønsted acids.[10, 11] These acids react with even the most inert solvents (e.g. liquid SO_2, alkanes, etc.), contrasting these Brønsted acids from more typical liquid superacids containing mixtures of HX and Lewis acids.[12] Reed described a clever strategy to assess Brønsted acid strength by measuring ν_{NH} of $[Oct_3N-H][X]$ in CCl_4 solution.[13] The apolar solvent promotes contact ion-pair formation, thus the ν_{NH} value correlates with ion-pair strength; weaker ion-pairs will have high ν_{NH} values and correlate with stronger acidity. Indeed, there is a linear correlation between ν_{NH} of $[Oct_3N-H][X]$ and DPE from DFT calculations across a wide range of anions, though calorimetry data that would deliver $\Delta H_{ion-pair}$ was not reported.

However, the challenge becomes more complex because many oxides containing Brønsted acidic –OH groups also contain Lewis sites that react with common bases used to probe these surfaces.[14] Indeed, strong Lewis acid sites are common on oxide surfaces and have important roles as heterogeneous catalysts.[15, 16]and are known to activate inert C–H bonds.[17-23]

Acidity is also practically important when reacting organometallics with oxides to form well-defined heterogenous catalysts.[23-28] Predicting which of the three structures would form in Figure 3 is straightforward, only if the types of reactive sites on an oxides are known. Oxides containing weak Brønsted acid –OH sites will react with $L_nM–R$ to form **A** while strong Brønsted acid –OH sites will form **B**. Alkyl or hydride abstraction reactions occur in reactions of organometallics and oxides containing a significant quantity of Lewis sites to form **C**. Though less common, this reaction is an important method to generate ion-pairs on surfaces.[29]
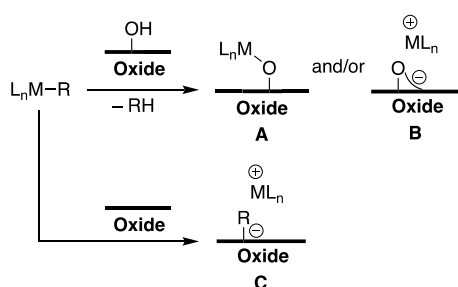

Figure 3. Reactions of $L_nM–R$ with an oxide can form neutral **A** or ion-paired **B** or **C.**

This article describes how Brønsted and Lewis acidity on surfaces affects the speciation shown in Figure 3, with an emphasis on generation of ion-pairs. We begin with a short description of molecular olefin polymerization catalysts because the activity of these complexes often depends on strong Brønsted and Lewis acid activators that form weakly coordinating anions that are critical for activity in this class of catalyst.[30] Using this reaction as motivation we also describe methods to generate well-defined strong Brønsted and Lewis acids on oxide surfaces that function as weakly coordinating oxides, which are an emerging class of supports that can have impact

on well-defined catalysts beyond olefin polymerization catalysis. An ever-present challenge in these studies is the characterization of the active site at the molecular level. This usually requires a combination of experimental spectroscopies. For example, rich molecular information is available using solid-state NMR spectroscopy,[31] and the advent of dynamic nuclear polarization (DNP)[32, 33] overcomes the low inherent sensitivity of NMR spectroscopy. When used in combination with computational studies[34] that correlate structure with the trends in NMR properties excellent structural resolution is possible. X-ray absorption spectroscopy is also commonly used to characterize these types of materials,[35] but care must be taken to correlate XAS properties with a library of carefully chosen molecular precursors.[36]

The Importance of Acidity on Surfaces in Heterogeneous Olefin Polymerization Catalysts

Catalysts that generate polyolefin plastics, extremely versatile materials produced on massive scales, are some of the most efficient and selective examples of catalysts in organometallic chemistry. This is in no small part due to the detailed mechanistic understanding of how these catalysts form and function in solution. The preceding decades saw tremendous advances in the design of transition metal catalysts for the polymerization of olefins,[30, 37-45] which continue to advance to address key challenges associated with the synthesis of state-of-the-art plastics.[46] These success stories are certainly related to systematic modification of simplified structural models to achieve a target property, Figure 4a.

In the most basic form, an active catalyst for olefin polymerization contains an empty coordination site *cis* to a metal-alkyl (or metal-hydride) of a usually cationic organometallic complex. The open coordination site and/or charge is installed using activators that suit either the early metal catalysts shown in Figure 4b or the late metal catalysts shown in Figure 4c. The vast majority of polymers generated industrially use Group IV organometallic cations, usually formed *in-situ* using organoaluminum activators, in the presence of strong Lewis acid (e.g. $B(C_5F_5)_3$, oxide, methaluminoxane).[30, 47] One exquisite set of examples showing how discrete control of the stereochemical environment of the active $Zr–R^+$ site result in different polypropylene products is shown in Figure 4b,[38] and relies on the formation of an ion-pair containing a weakly coordinating anion (e.g. $[MeB(C_6F_5)_3]$, $[B(C_6F_5)_4]$, $[MeAlO_X]$, etc.) for catalytic activity.
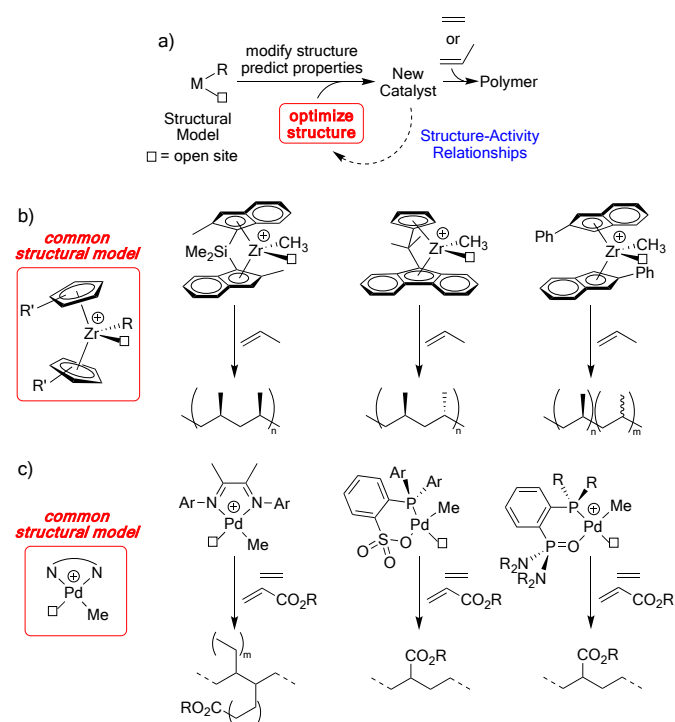
Figure 4. The structure activity relationship in olefin polymerization catalysts (a). Examples showing how the common $Cp_2Zr–R^+$ motif can be extended to complex structures that exert diastereocontrol in polypropylene synthesis (b). A related $(N^\wedge N)Pd–Me^+$ ($N^\wedge N$ = bidentate nitrogen containing ligand) structural model that results in polar monomer incorporation (c).

Late transition metal catalysts are often activated by solvated ether acid ($[HOEt_2][BAr_4]$, Ar = C_6F_5[48] or $3,5-(CF_3)_2-C_6H_4$[49]). The organopalladium catalysts shown in Figure 4c follow a similar structural model, but engage in different structure property trends because palladium catalysts can incorporate polar monomers into polyethylene chains. The α-diimine palladium catalysts reported by Brookhart and co-workers polymerize mixtures of ethylene and acrylate esters to incorporate the polar monomer into chain ends,[50] and manipulation of the aryl group on the ligand can modulate branching in the polymer.[51] However, the neutral phosphine-sulfonate palladium catalyst incorporates acrylate esters in-chain because these catalysts undergo slow chain-walking processes that creates branches.[40] The cationic phosphine-phosphine oxide catalyst essentially combines these two design strategies to form an electron rich palladium cation that produces linear copolymers that incorporate polar monomer in the PE chain.[52]

How do these trends apply to heterogeneous catalysts? The structure-property trend shown in Figure 5a, from a molecular chemist's point of view, is essentially broken for heterogeneous catalysts because of the challenges in assessing active site structure in these very complicated materials (Figure 5a). Indeed, a proposed intermediate for the "classic" Ziegler-Natta catalyst ($TiCl_4/AlR_3/MgCl_2$) was only recently detected using advanced EPR methods, Figure 5b.[53] More modern heterogeneous catalysts rely on mixtures of zirconocenes, alkylaluminums (or methaluminoxane[47]) and an oxide.[54] Based on the clear evidence from solution catalysts shown above, these likely form organometallic zirconocenium ion-pairs, Figure 5c. Applying a

similar strategy to heterogeneous Pd catalysts for olefin polymerization is not practical because common organoaluminum compounds are incompatible with most palladium precursors.[55]
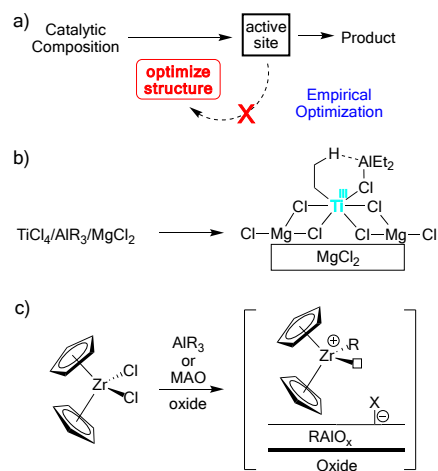

Figure 5. Empirical optimization for heterogeneous olefin polymerization catalysts resulting from poor structural knowledge of the active site (a). A plausible intermediate in classic Ziegler-Natta polymerization catalysts detected by EPR spectroscopy (b). Common mixtures used industrially that likely form $Cp_2Zr–R^+$ species on AlR_3 functionalized supports.

This is where acidity of surfaces emerges as an important factor in active site formation. We studied a model for industrial catalysts containing $Cp^b_2ZrCl_2$ (Cp^b = 1-butylcyclopentadienyl) in the presence of excess Al^iBu_3 and γ-alumina partially dehydroxylated at 600 °C.[56] The complex reactivity of this mixture shown in Figure 6 is required for self-assembly of the active site, and hinges on the promiscuity of the excess Al^iBu_3 in this mixture. First, Al^iBu_3 reacts with accessible –OH sites present on the γ-alumina surface. This reaction is critical because Al^iBu_3 also rapidly reacts with $Cp^b_2ZrCl_2$ to form mixtures of $Cp^b_2Zr(\mu-H)_3(Al^iBu_2)Al^iBu_3$ and $Cp^b_2Zr(\mu-H)_3(Al^iBu_2)_3(\mu-Cl)_2$ that would undoubtedly react with –OH sites on alumina to form inactive zirconium species. The latter reaction of Al^iBu_3 and unbridged zirconocenes appears general, but Zr(II) intermediates form with *ansa*-metallocenes resulting in complex speciation in solution.[57] After Al^iBu_3 performs these necessary tasks only $Cp^b_2Zr(\mu-H)_3(Al^iBu_2)Al^iBu_3$ reacts with residual Lewis sites on the passivated γ-alumina surface to form $[Cp^b_2ZrH][HAlO_X]$ ion-pairs. This reactivity is akin to the well-known reactions of Cp_2ZrMe_2 with the strong Lewis acid $B(C_6F_5)_3$ to form $[Cp_2ZrMe][MeB(C_6F_5)_3]$ ion-pairs in solution,[30] and related to classic examples describing how organometallics react with γ-alumina surfaces.[29, 58]

Figure 6. The network of reactions that occur to form active Cp^b_2Zr–H^+ sites on Al^iBu_3/Al_2O_3 surfaces.

Similar reactivity is not possible on Al^iBu_3/silica[54, 59] because this support lacks sufficient Lewis acidity to activate the *in-situ* generated $Cp^b_2Zr(\mu-H)_3(Al^iBu_2)Al^iBu_3$. However, relating the reactivity in Figure 6 to any Cp_2ZrCl_2/AlR_3/oxide combination should be taken with extreme caution. Though $Cp^b_2ZrCl_2/Al^iBu_3$/silica is not an active catalyst, zirconocene dichlorides with methaluminoxane and silica (or alumina[60]) are another common mixture for active olefin polymerization catalysts. Determining structure in the latter combination are exceptionally challenging because of the complexities associated with the behaviour of methaluminoxane in solution and on oxide surfaces.

Installing an Aluminum Lewis Site on Silica

The reactivity in Figure 6 clearly implicates that Al^iBu_3/alumina contains strong Lewis acid sites and that the $[H–AlO_X]$ anion behaves as a weakly coordinating anion.[61] Installing a strong Lewis site on an oxide to form a well-defined site is a surprising challenge. Partially dehydroxylated silica nearly always reacts with AlR_3[59, 62, 63,64] or GaR_3[65-67] to form mixtures of surface species. $B(C_6F_5)_3$ shows complicated reactivity with silica supports, Figure 7a. Reactions with silica pre-treated at 700°C (SiO_{2-700}, ~1 –OH nm²) form unstable adducts with isolated silanols and the borane, which can be deprotonated with aniline bases to form $[PhNHMe_2][\equiv SiOB(C_6F_5)_3]$.[68, 69, 70] However, silica pre-treated at 500 °C (SiO_{2-500}) reacts with $B(C_6F_5)_3$ through a series of steps to form pairs of $\equiv SiOB(C_6F_5)_2$ sites that are not capable of activating Cp_2ZrMe_2.[71]

$C_Q = 18.7$ MHz

Figure 7. Reactions of $B(C_6F_5)_3$ with SiO_2 (a). Differences in

transition state structure for the reaction of $B(C_6F_5)_3$ or $Al(OC(CF_3)_3)$ with SiO_2 (b).

We investigated the reaction of $Al(OC(CF_3)_3)(PhF)$[72] with SiO_{2-700}.[73] The choice of this particular combination was driven by two complementary rationales. First, $Al(OC(CF_3)_3)(PhF)$ is a significantly stronger Lewis acid than $B(C_6F_5)_3$ based on fluoride ion affinity calculations.[74, 75] Second, the Al–O in $Al(OC(CF_3)_3)(PhF)$ should be more reactive to the isolated silanols than the B–C in $B(C_6F_5)_3$. In both cases the Lewis acid coordinates to the silanol to form a bridging silanol intermediate (Figure 7b), which is certainly plausible for $B(C_6F_5)_3$ based on the reactivity shown in Figure 7a (top reaction) and was fully characterized in reactions of SiO_{2-700} and $Al(OC(CF_3)_3)(PhF)$,[76] which will be described in more detail in the section describing Brønsted acidity. In the transition state that results in grafting onto SiO_{2-700} the acidic proton is either transferred to the B–C to form $\equiv SiOB(C_6F_5)_2$ and C_6F_5H, which is evidently high barrier, or to the Al–O to form $\equiv SiOAl(OC(CF_3)_3)_2(O(Si\equiv)_2)$ and $HOC(CF_3)_3$. The fact that $\equiv SiOAl(OC(CF_3)_3)_2(O(Si\equiv)_2)$ forms and $\equiv SiOB(C_6F_5)_2$ does not is similar to results showing that $Zr(O^tBu)_4$ reacts with silica faster than $Zr(CH_3^tBu)_4$ despite the obvious thermodynamic driving force for the latter.[77]

The ^{27}Al MAS NMR spectrum of $\equiv SiOAl(OC(CF_3)_3)_2(O(Si\equiv)_2)$ acquired at 18.8 T shown in Figure 8a contains a signal at 74 ppm with a quadrupolar coupling constant (C_Q) of 18.0 MHz, consistent with a distorted trigonal bipyramidal Al environment ($\tau = 0.63$) that is reproduced using the small cluster model shown in Figure 8b. Fluoride ion affinity (FIA) calculations using typical isodesmic reactions[74,75] show that $\equiv SiOAl(OC(CF_3)_3)_2(O(Si\equiv)_2)$ has a FIA of 528 kJ mol^{-1}. This value is significantly larger than the calculated FIA for $B(C_6F_5)_3$ (448 kJ mol^{-1}) and slightly larger than isolable $Al(OC(CF_3)_3)(PhF)$ (514 kJ mol^{-1}), but less than a hypothetical free $^iPr_3Si^+$ (1073 kJ mol^{-1}).[78]

Figure 8. $^{27}Al\{^1H\}$ MAS NMR spectrum of $\equiv SiOAl(OC(CF_3)_3)_2(O(Si\equiv)_2)$ at 18.8 T (a, experimental in black simulation in red, $\nu_{rot} = 18.87$ kHz, * = probe background); calculated structures approximating $\equiv SiOAl(OC(CF_3)_3)_2(O(Si\equiv)_2)$ using a silsesquioxane cluster (b).[79] A structure showing the coordination environment around Al and the calculated ^{27}Al C_Q is given next to the calculated structure. Reproduced from ref. 76 with permission from Wiley-VCG GmbH, copyright 2022.

Cp_2ZrMe_2 reacts with $\equiv SiOAl(OC(CF_3)_3)_2(O(Si\equiv)_2)$ to form a mixture of surface species shown in Figure 9 indicative of methide abstraction, thus this material behaves similarly to $B(C_6F_5)_3$ in solution or solid Al^iBu_3/Al_2O_3. Unlike Al^iBu_3/Al_2O_3, which contains a very small quantity of Lewis sites (~ 0.65 μmol g^{-1} based on active Zr–H$^+$ quantification), the surface coverage of Lewis acidic Al in $\equiv SiOAl(OC(CF_3)_3)_2(O(Si\equiv)_2)$ is 240 μmol g^{-1}. This advantage will likely facilitate synthesis and characterization of other organometallic ion-pairs on this well-defined strong Lewis acid containing oxide.

Figure 9. The connections between Cp^bZrCl_2/Al^iBu_3/alumina, $B(C_6F_5)_3$ and $\equiv SiOAl(OC(CF_3)_3)_2(O(Si\equiv)_2)$ to form type **C** species.

Towards Weakly Coordinating Supports: The Importance of Brønsted Acidity

Brønsted acidic –OH sites, such as those present on sulfated oxides, form weakly coordinating ion pairs with organometallics.[80] The reactivity of $Cp*ZrMe_3$ with SiO_2 and sulfated aluminum oxide (**SAO**) serves as a representative example that distinguishes between type **A** and type **B** surface species, Figure 10. When supported on SiO_2 the organozirconium species formed, $Cp*ZrMe_2(OSi\equiv)$, is unreactive to ethylene polymerization because the necessary coordination site is "blocked" by the $^-OSi \equiv$ ligand.[81] However, **SAO** reacts with $Cp*ZrMe_3$ to form the $[Cp*ZrMe_2][SZO]$ ion-pair that is active for ethylene polymerization and arene hydrogenation reactions.[82, 83]
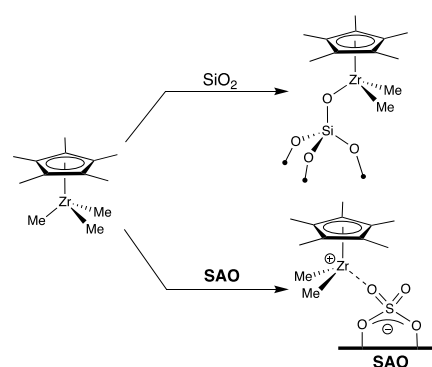

Figure 10. Reaction of $Cp*ZrMe_3$ with SiO_2 to generate $Cp*ZrMe_2(OSi\equiv)$ or sulfated aluminum oxide (**SAO**) to generate $[Cp*_2ZrMe][SZO]$.

Though the results in Figure 10 clearly implicate that **SAO** is a stronger Brønsted acid than SiO_2, the acid strength of sulfated oxides as a family of materials is controversial. For example, sulfated zirconium oxide (**SZO**) was reported to isomerize *n*-butane to isobutane at lower temperatures than 100 % H_2SO_4, which was interpreted as evidence for superacidic –OH sites on the ZrO_2 surface.[84] Subsequent colorimetric studies performed by adsorption of Hammett bases with known basicity onto **SZO** also suggested that the –OH sites on this support have H_0 values less than -16.04, suggesting that **SZO** is at least 4 orders of magnitude more acidic than 100 % H_2SO_4 ($H_0 = -12$).[85] As noted in the introduction, solid acids cannot be treated with similar methods as liquid acids, and colorimetric methods are not reliable measures of acid strength of solid acids.[86, 87] Indeed, several studies suggest that the Brønsted acid site has little, if any, influence on alkane isomerization chemistry of **SZO**.[88, 89]
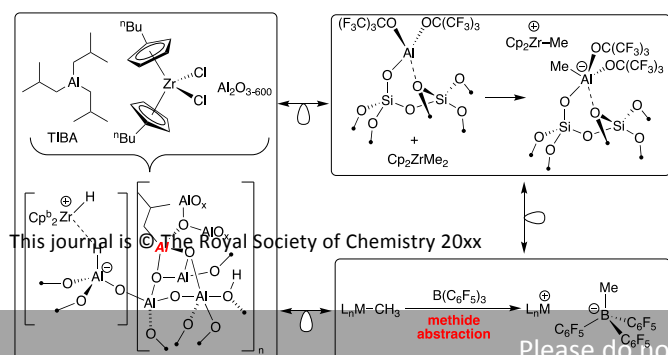
The **SZO** surface is complex and contains Brønsted,[90] Lewis,[91] and pyrosulfate sites;[92] selection of a probe molecule to evaluate only acidity of –OH sites is a challenge. We found that **SZO** partially dehydroxylated at 300 ºC reacts with P^{t}Bu$_3$ at 25 ºC in Et$_2$O to form only [HP^{t}Bu$_3$][**SZO**].[93] This result prompted us to systematically
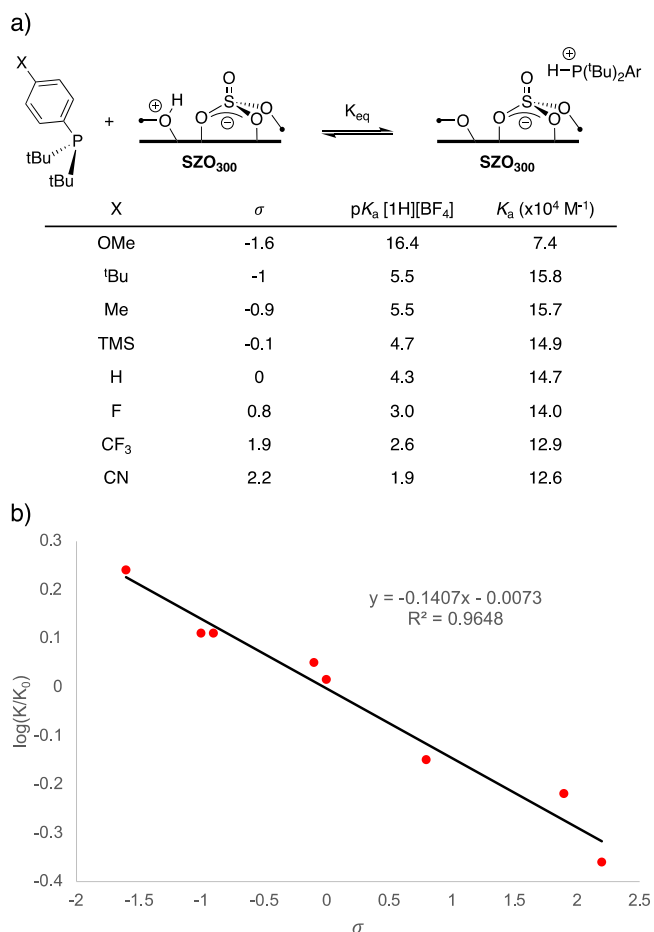
a)

X	σ	pK_a [1H][BF$_4$]	K_a (x10^4 M^{-1})
OMe	-1.6	16.4	7.4
^{t}Bu	-1	5.5	15.8
Me	-0.9	5.5	15.7
TMS	-0.1	4.7	14.9
H	0	4.3	14.7
F	0.8	3.0	14.0
CF$_3$	1.9	2.6	12.9
CN	2.2	1.9	12.6

b)

$y = -0.1407x - 0.0073$
$R^2 = 0.9648$

Figure 11. Reactions of ^{t}Bu$_2$PAr with **SZO** to form [(^{t}Bu)$_2$ArPH][**SZO**] in MeCN slurry (a). s, pK_a of [(^{t}Bu)$_2$ArPH][BF$_4$], and K_a for each substituent tested is given in the table below the equation. Hammett plot for the binding of ^{t}Bu$_2$PAr to **SZO** (b).

study the reaction of substituted ^{t}Bu$_2$PAr with **SZO** in MeCN to determine how electronics at phosphorus affect the formation of [(^{t}Bu)$_2$ArPH][**SZO**], Figure 11a. In all cases the adsorption equilibria follow classic Langmuir binding isotherms that allow for extraction of K_a for the range of [(^{t}Bu)$_2$ArPH][**SZO**] generated in this study. Binding to **SZO** ($19000 < K_a < 74000$ in MeCN) systematically decreases as the pK_a of [(^{t}Bu)$_2$ArPH][BF$_4$] increases over almost four orders of magnitude ($12.6 < pK_a < 16.4$ in MeCN). A Hammett plot of σ, derived from the pK_a of the [(^{t}Bu)$_2$ArPH][BF$_4$],[94] versus K_a is linear, Figure 11b. This particular result shows that Hammett behavior is possible for a solid acid once solvation is introduced.**Figure 11**. Reactions of ^{t}Bu$_2$PAr with **SZO** to form [(^{t}Bu)$_2$ArPH][**SZO**] in MeCN slurry (a). s, pK_a of [(^{t}Bu)$_2$ArPH][BF$_4$], and K_a for each substituent tested is given in the table below the equation. Hammett

plot for the binding of ^{t}Bu$_2$PAr to **SZO** (b).This behavior is inconsistent with superacidic behavior. First, MeCN reacts with superacids to form [H(MeCN)$_n$] solvates,[12] which is expected to result in significantly higher K_a values. Second, weaker bases like PPh$_3$ (pK_a(HPPh$_3$) = 7.6 in MeCN) have very low affinity for **SZO** ($K_a \sim 3$ M^{-1}), and p-nitroaniline (pK_a(anilinium) = 6.22 in MeCN)[95] does not react to form an ammonium on the **SZO** surface.

This study shows that **SZO** is, in fact, a rather weak Brønsted acid. Indeed, DFT calculations show that sulfuric acid adsorbs onto ZrO$_2$ surfaces to form tripodal sulfate sites with the proton laying on nearby Zr–O–Zr bridges.[96] The calculated DPE of the protonated Zr–O–Zr bridges ranges from 1339 – 1548 kJ mol^{-1}, significantly higher than the DPE of H$_2$SO$_4$ (1306 kJ mol^{-1}). This collection of results is satisfying because ZrO$_2$ is a mild proton acceptor (i.e. a Brønsted base), and it is not expected that the reaction of a strong acid and a weak base would result in a superacid.

Until recently, sulfated oxides were the only weakly coordinating support available to form ion-pairs with organometallics. This is a significant limitation considering the structural diversity and range of ion-pairing characteristics widely available to the community that uses weakly coordinating anions in solution.[97, 98] We approached this challenge by generating a very strong Brønsted acid site on an oxide. The Brønsted site in zeolites and silica alumina are silanols coordinated to a nearby Lewis acidic aluminum in the material framework, simplified in Figure 12a. We viewed this as a solid Lewis acid activated Brønsted acids that have extensive precedent in the synthetic organic chemistry community.[99] Selection of an appropriately strong Lewis acid should result in formation of a well-defined strong Brønsted acid site that when deprotonated should behave as a weakly coordinating anion.[100]
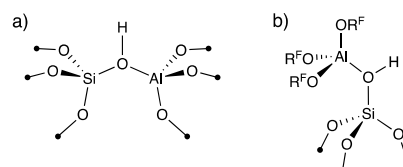

Figure 12. The acidic bridging silanol in a silica alumina (a) and in Al(OC(CF$_3$)$_3$)(PhF) reacted with SiO$_{2-700}$ to form ≡Si–OH---Al(OR^F)$_3$ (b).

The reaction of Al(OC(CF$_3$)$_3$)(PhF) with SiO$_{2-700}$ results in solvent specific reactivity. In PhF with mild heating ≡SiOAl(OC(CF$_3$)$_3$)$_2$(O(Si ≡)$_2$) forms as discussed above.[73] In perfluorohexanes at 25 ºC Al(OC(CF$_3$)$_3$)(PhF) reacts with SiO$_{2-700}$ to form the bridging silanol ≡Si–OH---Al(OR^F)$_3$, Figure 12b.[76] Al(OC(CF$_3$)$_3$) coordinated to an isolated silanol on a small cluster model reproduces ν_{OH} (exp = 3550 cm^{-1}, calc = 3542 cm^{-1}), ^{1}H NMR chemical shift (exp = 5.0 ppm, calc = 5.1 ppm), ^{27}Al NMR properties (exp C_Q = 14.6 MHz, calc C_Q = 15.3 MHz), and H–Al distance (exp = 2.4 – 2.5 Å, calc = 2.46 Å). The excellent agreement between experiment and theory provides foundation for the calculated DPE using this model, which was 1099 kJ mol^{-1}. At the same level of theory the DPE of HSO$_3$CF$_3$ is 1233 kJ mol^{-1} (exp = 1240 kJ mol^{-1}). Though ≡Si–OH---Al(OR^F)$_3$ is a strong Brønsted acid it is still far weaker than H[Al(OR^F)$_4$] (calc = 1041 kJ mol^{-1})[101] and H[CHB$_{11}$Cl$_{11}$] (calc = 1000 kJ mol^{-1}).[13]

The strong Brønsted acidity of $\equiv$Si–OH---Al(OR^F)$_3$ implies weakly coordinating behavior when deprotonated. The reaction of $\equiv$Si–OH---Al(OR^F)$_3$ with NOct$_3$ forms [HNOct$_3$][$\equiv$SiO–Al(OR^F)$_3$], which has a ν_{NH} at 3070 cm^{-1}. This value is higher than [ClO$_4$] (3049 cm^{-1}), [FSO$_3$] (2953 cm^{-1}), and [CF$_3$SO$_3$] (2939 cm^{-1}); but lower than [CHB$_{11}$Cl$_{11}$] (3163 cm^{-1}) and [B(C$_6$F$_5$)$_4$] (3223 cm^{-1}). These results indicate that [$\equiv$SiO–Al(OR^F)$_3$] is more weakly coordinated to the ammonium than first generation anions, but less weakly coordinated than state-of-the-art borane and carborane anions.

The Relationship Between ^{29}Si NMR Chemical Shift and Brønsted Acidity: An Emerging Scale for Solid-State Acidity?

The power of pK_a or Hammett acidity parameters are obvious. These values provide a direct method to compare a key thermodynamic driving force that predicts reactivity. A similar "single-point" measurement or parameter that predicts the Brønsted acidity of a solid acid would be similarly beneficial. From the discussion above, we tend to focus on calculated DPE as a reliable measure of acidity for solids because this is the only parameter that gives a measure for the thermochemical driving force for the heterolytic cleavage of an –OH to H$^+$ and –O$^-$. The drawback of this approach is that values obtained from these calculations depend on how accurately the model represents reality, which can be difficult when modelling surface species.

One of the most common methods to obtain information about acidity on a surface is to adsorb a probe that has a spectroscopic readout. The classic example is adsorption of pyridine onto an oxide, which has a characteristic $\nu_{C=C}$ stretch that is used to quantify Brønsted and Lewis site surface coverage.[102,6] Solid-state NMR spectroscopy of oxides contacted with probe molecules is another promising method to obtain information about acidity. Drago showed that adsorption of triethylphosphine oxide (TEPO) onto an oxide results in changes in ^{31}P MAS NMR chemical shift that correlates to some degree with Brønsted or Lewis acidity of surface sites.[103] The ^{31}P{^{1}H} NMR chemical shift of TEPO coordinated to a Lewis acid is also an excellent probe to measure Lewis acid strength.[104] Indeed, phosphorous probes are very useful probes for acidity because they are both Brønsted and Lewis bases, and the high sensitivity ^{31}P NMR nucleus allows for rapid signal acquisition.[5, 105]

The ^{29}Si NMR chemical shift of R$_3$Si-capped oxides is emerging as another single-point measurement that provides information about Brønsted acidity of –OH sites on oxides. The origin of deshielding in ^{29}Si NMR is related to the structure of R$_3$Si–X or [R$_3$Si][X].[106] For a planar "free" ^{i}Pr$_3$Si$^+$, which has resisted isolation even with the most weakly coordinating anions,[107, 108] DFT calculations predict a ^{29}Si NMR chemical shift of 343 ppm. The ^{29}Si NMR chemical shift of [^{i}Pr$_3$Si][CH$_6$B$_{11}$Br$_6$] is 110 ppm, and data from single crystal X-ray diffraction studies show that the Si is pyramidal (Σ_{C-Si-C} = 350.9^o) because a Br from the carborane anion is in close contact to the Lewis acidic silicon.[109] DFT reproduces this structure and ^{29}Si NMR chemical shift, and broadly reproduces these parameters for a wide range of R$_3$Si–X or [R$_3$Si][X].

^{29}Si NMR chemical shift deshielding is related to the paramagnetic term (σ^p) of the isotropic chemical shift (σ^{iso}). The magnitude of σ^p is proportional to the coupling between the ground state wavefunction (φ_0) and an excited state wave- function (φ_n) through the angular

momentum operator ($\hat{L}_{ki}$, where ki = element of the shielding tensor, eq 1). The denominator in Eqn (1) shows that large σ^p contributions are also expected when φ_0 and φ_n are close in energy, which is maximized at the HOMO – LUMO gap. This effect is largest for the σ_{11} component of the chemical shift tensor, which is reliably calculated using DFT methods, and has found broad application to predict structure and reactivity in organometallic compounds,[110-112] organic molecules,[113] and aryllithium reagents.[114]

$$\sigma_{ij}^p \propto \frac{\left\langle\varphi_0\left|\hat{L}_{ki}\right|\varphi_n\right\rangle\left\langle\varphi_n\left|\dfrac{\hat{L}_{kNj}}{r_{kN}^3}\right|\varphi_0\right\rangle}{\Delta E_{n-0}} \quad (1)$$

Figure 13 shows the surface of the chemical shift tensor (CST), the orientation of the CST, and the orbitals involved in σ^p for planar ^{i}Pr$_3$Si$^+$ and pyramidal [^{i}Pr$_3$Si][CH$_6$B$_{11}$Br$_6$]. In both cases the HOMO is the σ_{Si-C} and the LUMO is the formally empty p-orbital on silicon. In anion-free ^{i}Pr$_3$Si$^+$ the planar silicon places the σ_{Si-C} perpendicular to the LUMO, which results in strong paramagnetic deshielding and large σ^p. Approach of the weak [CH$_6$B$_{11}$Br$_6$] nucleophile results in pyramidalization at silicon, which reduces σ^p and results in a less deshielded ^{29}Si NMR nucleus.
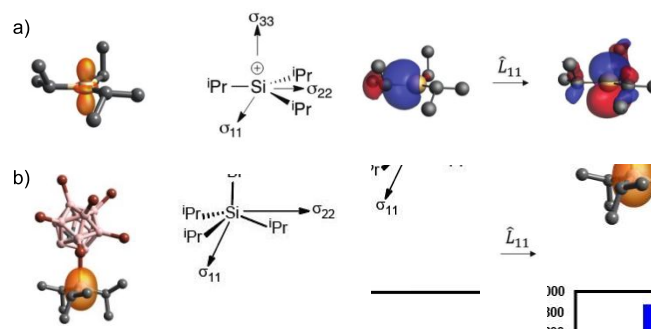

Figure 13. Surface of the CST using TensorView,[115] orientation of the CST, and orbitals involved in σ^p of the most deshielded (σ_{11}) term of the CST that result in the downfield chemical shift for ^{i}Pr$_3$Si$^+$ (a) and [^{i}Pr$_3$Si][CH$_6$B$_{11}$Br$_6$] (b). Reproduced from ref. 106 with permission from the Royal Society of Chemistry, copyright 2020,

There is a reasonable correlation between DPE and ^{29}Si NMR chemical shift, Figure 14a. This trend is related to the pyramidalization at silicon and not charge, the latter of which is not expected to affect chemical shift.[116] Importantly, this correlation is applicable over a broad range of DPE for both molecular HX and small clusters that approximate the chemical environment of R$_3$Si-capped surfaces. The three small clusters shown in Figure 13b approximate the isolated silanol on silica (DPE = 1503 kJ mol^{-1}),[117] the acidic bridging silanol in $\equiv$Si–OH---Al(OR^F)$_3$, and the –OH on **SZO** (DPE = 1188 kJ mol^{-1}). The acidic $\equiv$Si–OH---Al(OR^F)$_3$ and **SZO** supports react with allyltriisopropylsilane to form the corresponding [^{i}Pr$_3$Si][oxide] ion-pairs.[76, 118]
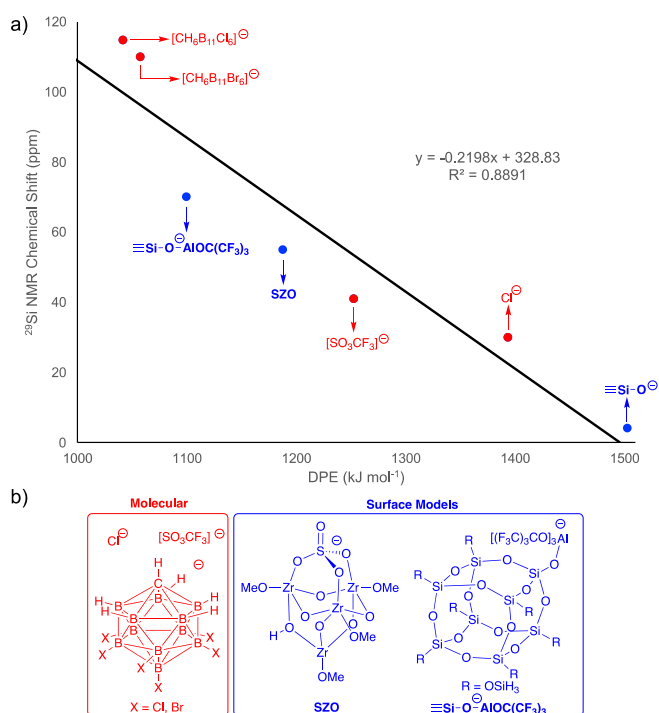
Figure 14. Plot of DPE of HX versus ^{29}Si NMR chemical shift (a). Structures of the anions (b).

The four molecular anions shown in Figure 14 span ~350 kJ mol^{-1} in DPE. As the anion becomes less basic (i.e., HX becomes more acidic) the ^{29}Si NMR chemical shift appears more downfield. Silanols on silica are weak acids. Thus, the shielded ^{29}Si chemical shift values for R_3Si-supported on silica appear (~4 ppm)[119-121] as expected. As the DPE of the –OH group on the support decreases the ^{29}Si NMR chemical shift also increases. These trends are very similar to those found by Reed in studies that resulted in the ν_{NH} scale with [Oct$_3$NH][X].[13]

To our knowledge H-Beta treated with PhSiMe$_3$ is the only example of a Me$_3$Si-functionalized zeolite, which has a ^{29}Si NMR signal at 17 ppm for the organosilane.[122] This result would seem to break the line shown in Figure 14 because zeolites should behave as strong Brønsted acids. However, it is not clear which –OH groups in H-Beta react with PhSiMe$_3$, and the strong Brønsted acid bridging silanol in micropores may not be accessible to PhSiMe$_3$.

Weakly Coordinating Oxides in Olefin Polymerization Reactions
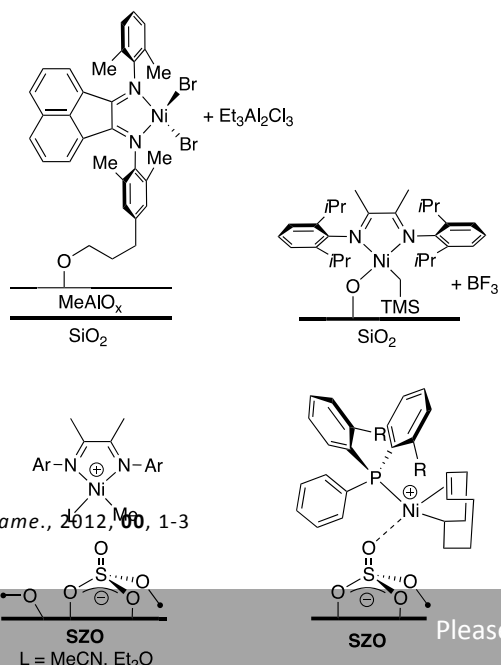
common mixture to generate heterogeneous catalysts for olefin polymerization contains a metallocene, an alkylaluminum (or MAO), and an oxide. This method is broadly applicable to group IV metals, but less so for late transition metal olefin polymerization catalysts. Figure 15 shows examples of heterogeneous (α-diimine)Ni catalysts. Combinations of (α-diimine)NiBr$_2$ containing a pendant –OH group on the ligand, SiO$_2$/MAO, and exogenous Et$_3$Al$_2$Cl$_3$, are active in ethylene polymerization but the broad molecular weight polymer formed in this reaction is a hallmark of ill-defined active sites.[123] Well-defined catalysts containing (α-diimine)Ni(CH$_2$SiMe$_3$)$_2$ grafted onto SiO$_{2-700}$ show modest activity in the presence of BF$_3$.[124]

Figure 15. Heterogeneous Ni complexes for olefin polymerization.

Sulfated oxides are ideal candidates to form well-defined heterogeneous catalysts for olefin polymerization because these are sufficiently weakly coordinating to form the requisite organometallic ion-pair that fulfills the
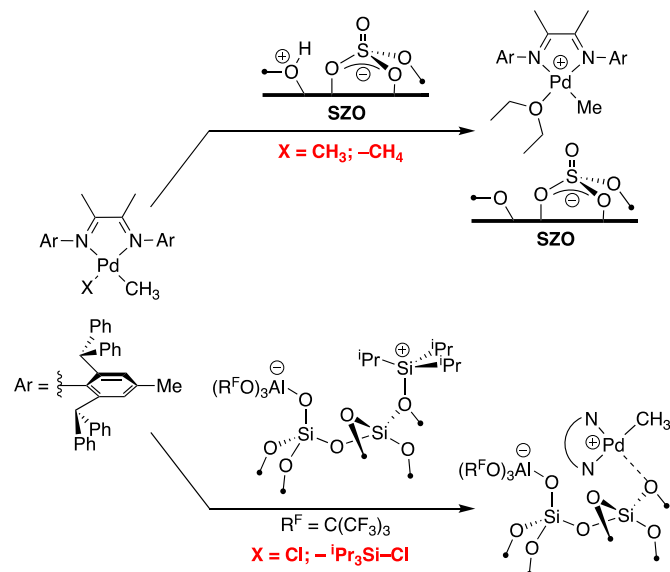
requirements for the basic structural model shown in Figure 4. Reactions of an (α-diimine)NiMe$_2$ with **SZO** generate well-defined Ni–Me$^+$ sites, all of which are active in olefin insertion reactions, which produce narrow molecular weight polymers and can tolerate polar monomers.[125] Active catalysts are also available containing organozirconium[126] or organohafnium[127] complexes supported on sulfated oxides, showing that this strategy is general for reactions of M–R with sulfated oxides to form polymerization complexes. [HPAr$_3$][**SZO**] prepared similarly to those discussed above react with Ni(cod)$_2$ to form [Ni(PAr$_3$)(codH)][**SZO**] that are also reactive in olefin polymerization reactions,[128] showing that complex catalyst architectures are likely possible on sulfated oxides.

However, even general reactions have pitfalls. The reaction of the bulky (α-diimine)PdMe$_2$[129, 130] shown in Figure 16 reacts with **SZO** to form a well-defined Pd–Me$^+$ site.[131] This reaction is also accompanied by significantly more CH$_4$ than expected, indicating that some Pd sites lack the alkyl group necessary for polymerization. Indeed, active site counting shows that only ~9 % of the Pd is active in polymerization reactions. Accessing heterogeneous Pd catalysts for olefin polymerization is generally difficult because of incompatibilities with AlR$_3$, preventing use of common mixtures for catalyst generation, and for the undesirable reactivity shown in Figure 16 between (α-

diimine)PdMe₂ and **SZO**. The only other two other examples involved supported phosphine sulfonate Pd species,[132] or anilinonapthoquinone Pd-complexes adsorbed onto silica were known.[133]

We showed that [^{i}Pr$_3$Si][≡SiO–Al(OR^F)$_3$] reacts with (α-diimine)PdMeCl by a halide abstraction route that forms [(α-diimine)PdMe][≡SiO–Al(OR^F)$_3$], Figure 16.[134] This reaction is very selective (^{i}Pr$_3$SiMe is not detected) because R$_3$Si$^+$ ions have some of the highest halide ion affinities known.[108] In addition virtually all of the Pd–Me$^+$ sites are active in olefin insertion reactions. Halide abstraction is a general methodology to generate ion-pairs in solution,[45, 61] and we view this reaction as filling a methodological gap in the surface organometallic community that often relies on reactions of Brønsted acid sites with organometallics to form well-defined species.

Figure 16. Heterogeneous Pd catalysts for olefin polymerization prepared by traditional protonolysis methods (top) or recently developed halide abstraction (bottom).

Beyond Olefin Polymerization with Supported Organometallic Cations

Reactive d^0 metal hydrides have a rich history as well-defined heterogenous catalysts supported on SiO$_2$,[135, 136] usually prepared by treating supported organometallics with H$_2$. Silica-supported late transition metal hydrides on supports are less common,[137-139] but can be prepared by oxidative addition of Pt(0) to generate Pt–H species.[140] Though reactive, –OH groups on SiO$_2$ nearly always favor formation of type **A** species containing ≡SiO–M (Figure 3).[141]

Figure 9 showed differences in the reactivity of Cp*ZrMe$_3$ with SiO$_2$ and **SAO**, the latter forming an ion pair that has activity in olefin polymerization reactions. Contacting the [Cp*ZrMe$_2$][**SAO**] forms very reactive Zr–H$^+$ species that hydrogenate arenes, Figure 17.[82, 83, 142, 143] The key step in this reaction is the coordination of the arene to the electron deficient Zr–H$^+$, which can be thought of as a surface analog to a solvent separated ion pair. This behavior is analogous to cationic d^0 species that coordinate and exchange arene solvents in solution.[144-146] Successive migratory insertion and hydrogenolysis steps shown in Figure 17 form the cyclohexane product. This reaction shows remarkable facial selectivity, giving all *cis*-substituted products in hydrogenation reactions of substituted arenes.[147]
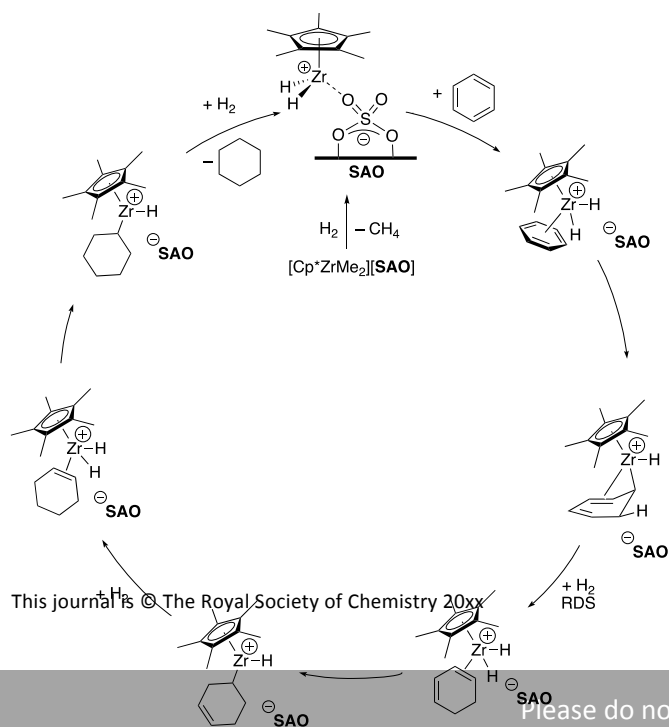
Figure 17. Arene hydrogenation of catalyzed by Zr–H$^+$ supported on **SAO**.

Most of the classic examples of d^0 M–H supported on silica engage in σ-bond metathesis reactions.[135, 136] Zr–H/SiO$_2$ are promising catalysts for hydrogenolysis of polyethylene,[148] which is attracting increasing attention as a method to degrade polymer waste to useful alkane feedstocks.[149] One of the many challenges in this chemistry is the slow reaction kinetics resulting in long reaction times. In alkane hydrogenolysis Zr–H reacts with a C–H bond through σ-bond metathesis to form H$_2$ and M–R that β-alkyl eliminates[150] to form MR(olefin) intermediates that are successively hydrogenated to lower molecular weight products, Figure 18. Though the rate limiting step in this reaction is not known, in solution cationic d^0 organometallics react faster in σ-bond metathesis reactions than related neutral species,[151] suggesting that d^0 M–H$^+$ may accelerate alkane rearrangements.[152]
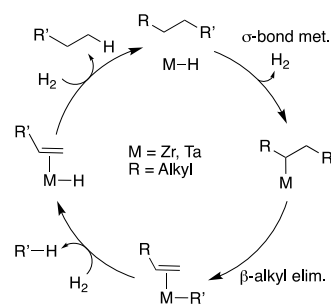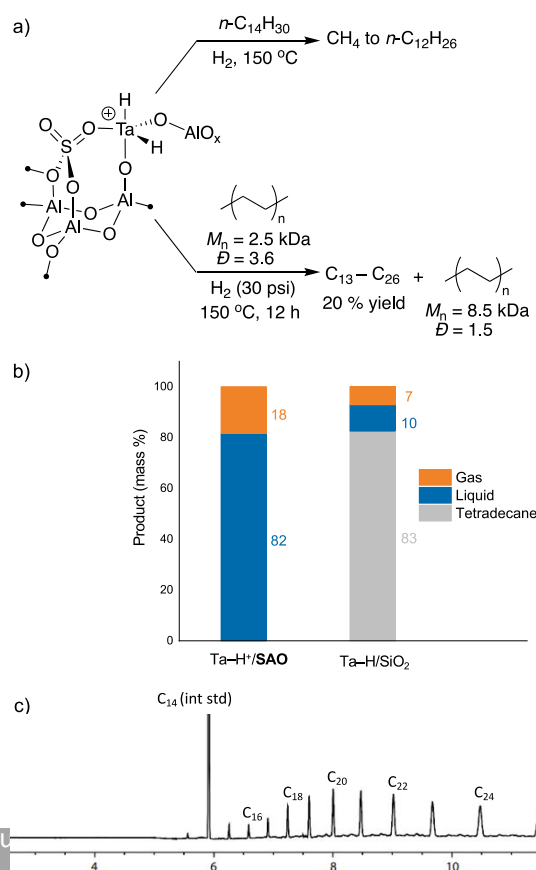
Figure 18. Alkane hydrogenolysis by a M–H.

We prepared Ta–H$^+$ sites on **SAO** (Figure 19a)[153] and compared their reactivity to Ta–H supported on SiO$_2$, the latter of which are known to catalyze alkane hydrogenolysis reaction.[154] Ta–H$^+$ sites on **SAO**

converts 100 equivalents of *n*-C$_{14}$H$_{30}$, a liquid surrogate for polyethylene, to a statistical mixture of alkanes in only 2h, while identical reaction conditions with Ta–H supported on SiO$_2$ results in only 17% conversion of tetradecane. Ta–H$^+$ sites on **SAO** also catalyze hydrogenolysis of low molecular weight HDPE to produce C$_{13}$ − C$_{26}$ in 20 % yield. The residual polymer has higher molecular weight than the starting material suggesting that only the more mobile polymer fraction reacts with Ta–H$^+$ sites on **SAO**. Finally, Ta–H$^+$ sites on **SAO** are also significantly more reactive in alkane metathesis reactions than Ta–H supported on SiO$_2$.

Figure 19. Reactivity of Ta–H$^+$ on **SAO** in hydrogenolysis reactions (a). Direct comparison of Ta–H$^+$/**SAO** and Ta–H/SiO$_2$ in tetradecane hydrogenolysis after 2 h (b). Gas chromatograph of products produced by Ta–H$^+$/**SAO** in hydrogenolysis of polyethylene. Reproduced from ref. 153 with permission from the American Chemical Society, copyright 2023.

Designing cationic metal hydrides on weakly coordinating supports appears to be a promising strategy to increase reactivity in alkane rearrangement reactions. Similar strategies using cationic transition metal complexes in solution to mediate these reactions are unlikely for a simple reason, alkanes are rarely compatible solvents with cations. Indeed, solvation of organometallic cations by polar halogenated solvents usually prevents formation of σ-CH alkane intermediates in solution,[155-159] and only recently have these types of compounds become widely available in using *in-crystallo*[160] organometallic chemistry of cationic Rh(I) olefin complexes with H$_2$ in porous single crystals in the absence of solvent.[161-166]

This concept extends beyond generation of M–H$^+$ sites on weakly coordinating supports. [Cp*IrMe(PMe$_3$)][**SZO**] in Figure 20a catalyzes H/D exchange reactions of methane and arenes faster than the corresponding Ir species supported on SiO$_2$.[167] This reaction is mechanistically similar to the σ-bond metathesis reactions discussed above,[168] but shows that trends observed in supported d^0 species also extend to Ir. C–H activation reactions that involve concerted metalation deprotonation (CMD)[169] are also accelerated on weakly coordinating supports. Cationic (*dm*Phebox)Ir(III) (Figure 20b) supported on **SZO** is more active in stoichiometric dehydrogenation reactions than the corresponding neutral complex in solution.[170] DFT studies support experimental observations and show that neutral (*dm*Phebox)Ir(OAc)$_2$ is predicted to activate C–H bonds with higher barrier to produce more stable intermediates than [(*dm*Phebox)Ir(OAc)][**SZO**]. This also results in higher barrier for β-H elimination, a key step in Ir-catalyzed dehydrogenation reactions,[171] for the neutral Ir–R compared to the cationic supported species.
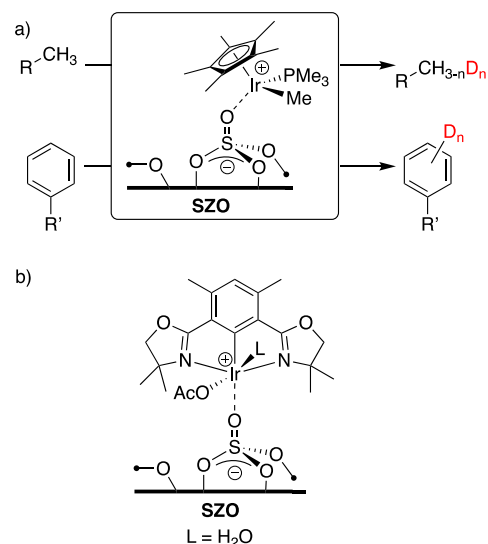

Figure 20. H/D exchange of arenes and alkanes catalyzed by [Cp*IrMe(PMe$_3$)][**SZO**] (a). Cationic [(*dm*Phebox)Ir(OAc)][**SZO**] (b).

Outlook

Acidity plays a deciding role in the structure of organometallics on surfaces. Though quantification of Brønsted and Lewis acidity on surfaces cannot directly parallel trends observed in solution, this article showed various methods that can provide key insights to acid strength on surfaces. Titrations of –OH groups on supports are possible, as shown for reactions of PR$_3$ with **SZO**, but laborious. We feel that the relationship between ^{29}Si NMR chemical shift and DPE is a more powerful single point measurement that reports on the ability of an oxide to form an ion-pair. This is because of the broad ^{29}Si NMR chemical shift window between R$_3$Si–X, R$_3$Si$^{\delta+}$•••$^{-\delta}$X, and [R$_3$Si][X]. The ^{29}Si NMR chemical shift is predicted to vary ~300 ppm between R$_3$Si–OMe and free R$_3$Si$^+$ (R = alkyl). Though the formation of a free R$_3$Si$^+$ on an oxide is unlikely the practical range in ^{29}Si NMR chemical shift scale is closer to ~100 ppm using R$_3$Si–OMe and [R$_3$Si][CH$_6$B$_{11}$Cl$_6$] as examples. This spans a wide range of DPE; the acidic end of this range of DPE being significantly lower than ≡Si–OH---Al(OR^F)$_3$, the strongest Brønsted acid on an oxide and the most weakly coordinating oxide from the ^{29}Si NMR chemical shift scale.

Access to more weakly coordinating supports remains a significant challenge. The Lewis activated Brønsted acid strategy is promising, but still in in its infancy on heterogeneous supports. Part of this reason is related to the need for stronger Lewis acids that bind to –OH groups on surfaces with sufficient binding energy to form a bridging ≡E–OH---LA site (E = surface element). Lewis acids stronger than Al(OR^F)$_3$, which are becoming available,[172] would be useful for this purpose. The alternative is to react oxides containing stronger Brønsted acid – OH groups with Al(OR^F)$_3$(PhF) to enhance acidity.

The use of the ^{29}Si NMR chemical shift scale has a hidden benefit. Weakly coordinating oxides form R$_3$Si$^+$ capped surfaces that show characteristic reactivity of silylium-like ions. [R$_3$Si][**SZO**] activate C–F bonds[118] or abstract chloride from (cod)IrCl(py).[173] R$_3$Si$^+$ have exceptionally high halide ion affinities, indicating that R$_3$Si$^+$ capped surfaces will selectively abstract a halide from an organometallic

complex, as shown for the reaction of (N^N)PdMeCl with [¹Pr₃Si][≡SiO–Al(OR^F)₃] in Figure 16.

As the field of surface organometallic chemistry continues to grow more nuanced methods to evaluate how the support affects structure will likely be necessary. Acidity clearly plays a deciding role in the species described here, but there are supports, such as redox active battery materials,[174] where new metrics will be needed to accurately describe how thermodynamics properties of the surface affects structure of an organometallic or inorganic site active in a catalytic reaction.

Author Contributions

Both authors contributed to the preparation of this manuscript.

Conflicts of interest

There are no conflicts to declare.

Acknowledgements

Notes and references

1. R. H. Morris, *Chem. Rev.*, 2016, **116**, 8588-8654.
2. Y. Marcus, M. J. Kamlet and R. W. Taft, *J. Phys. Chem.*, 1988, **92**, 3613-3622.
3. in *Ions in Solution and their Solvation*, 2015, DOI: https://doi.org/10.1002/9781118892336.ch4, pp. 107-155.
4. W. E. Dasent, *Journal*, 1983, **96**, 194-195.
5. A. Zheng, S.-B. Liu and F. Deng, *Chem. Rev.*, 2017, **117**, 12475-12531.
6. M. I. Zaki, M. A. Hasan, F. A. Al-Sagheer and L. Pasupulety, *Colloids and Surfaces A: Physicochemical and Engineering Aspects*, 2001, **190**, 261-274.
7. C. Morterra and G. Magnacca, *Catal. Today*, 1996, **27**, 497-532.
8. W. E. Farneth and R. J. Gorte, *Chem. Rev.*, 1995, **95**, 615-635.
9. R. J. Gorte, *Catal. Lett.*, 1999, **62**, 1-13.
10. C. A. Reed, *Acc. Chem. Res.*, 2013, **46**, 2567-2575.
11. C. A. Reed, *Acc. Chem. Res.*, 2010, **43**, 121-128.
12. G. A. Olah, G. K. S. Prakash, J. Sommer and A. Molnar, *Superacid Chemistry*, John Wiley & sons, 2009.
13. E. S. Stoyanov, K.-C. Kim and C. A. Reed, *J. Am. Chem. Soc.*, 2006, **128**, 8500-8508.
14. J. F. Haw, *Phys. Chem. Chem. Phys.*, 2002, **4**, 5431-5441.
15. A. Corma and H. García, *Chem. Rev.*, 2003, **103**, 4307-4366.
16. Y. Román-Leshkov and M. E. Davis, *ACS Catal.*, 2011, **1**, 1566-1580.
17. A. Comas-Vives, M. Valla, C. Copéret and P. Sautet, *ACS Cent. Sci.*, 2015, **1**, 313-319.
18. A. Comas-Vives, M. Schwarzwälder, C. Copéret and P. Sautet, *J. Phys. Chem. C*, 2015, **119**, 7156-7163.
19. M. Valla, R. Wischert, A. Comas-Vives, M. P. Conley, R. Verel, C. Copéret and P. Sautet, *J. Am. Chem. Soc.*, 2016, **138**, 6774-6785.
20. R. Wischert, C. Copéret, F. Delbecq and P. Sautet, *Angew. Chem., Int. Ed.*, 2011, **50**, 3202-3205.
21. R. Wischert, C. Coperet, F. Delbecq and P. Sautet, *Chem. Commun.*, 2011, **47**, 4890-4892.
22. C. Coperet, *Chem. Rev.*, 2010, **110**, 656-680.
23. C. Copéret, A. Comas-Vives, M. P. Conley, D. P. Estes, A. Fedorov, V. Mougel, H. Nagae, F. Núñez-Zarur and P. A. Zhizhko, *Chem. Rev.*, 2016, **116**, 323-421.
24. J. D. A. Pelletier and J.-M. Basset, *Acc. Chem. Res.*, 2016, **49**, 664-677.
25. S. L. Wegener, T. J. Marks and P. C. Stair, *Acc. Chem. Res.*, 2011, **45**, 206-214.
26. Y. Liang and R. Anwander, *Dalton Trans.*, 2013, **42**, 12521-12545.
27. J. Guzman and B. C. Gates, *Dalton Trans.*, 2003.
28. E. Bekyarova and M. P. Conley, *Dalton Trans.*, 2022, **51**, 8557-8570.
29. P. J. Toscano and T. J. Marks, *J. Am. Chem. Soc.*, 1985, **107**, 653-659.
30. E. Y.-X. Chen and T. J. Marks, *Chem. Rev.*, 2000, **100**, 1391-1434.
31. C. P. Gordon, L. Lätsch and C. Copéret, *The Journal of Physical Chemistry Letters*, 2021, **12**, 2072-2085.
32. A. J. Rossini, A. Zagdoun, M. Lelli, A. Lesage, C. Copéret and L. Emsley, *Acc. Chem. Res.*, 2013, DOI: 10.1021/ar300322x.
33. A. J. Rossini, *The Journal of Physical Chemistry Letters*, 2018, **9**, 5150-5159.
34. P. Sautet and F. Delbecq, *Chem. Rev.*, 2010, **110**, 1788-1806.
35. S. Bordiga, E. Groppo, G. Agostini, J. A. van Bokhoven and C. Lamberti, *Chem. Rev.*, 2013, **113**, 1736-1850.
36. D. Trummer, K. Searles, A. Algasov, S. A. Guda, A. V. Soldatov, H. Ramanantoanina, O. V. Safonova, A. A. Guda and C. Copéret, *J. Am. Chem. Soc.*, 2021, **143**, 7326-7341.
37. G. W. Coates, P. D. Hustad and S. Reinartz, *Angew. Chem., Int. Ed.*, 2002, **41**, 2236-2257.
38. G. W. Coates, *Chem. Rev.*, 2000, **100**, 1223-1252.
39. S. L. J. Luckham and K. Nozaki, *Acc. Chem. Res.*, 2021, **54**, 344-355.
40. A. Nakamura, T. M. J. Anselment, J. Claverie, B. Goodall, R. F. Jordan, S. Mecking, B. Rieger, A. Sen, P. W. N. M. van Leeuwen and K. Nozaki, *Acc. Chem. Res.*, 2013, **46**, 1438-1449.
41. Z. Chen and M. Brookhart, *Acc. Chem. Res.*, 2018, **51**, 1831-1839.
42. C. Tan and C. Chen, *Angew. Chem., Int. Ed.*, 2019, **58**, 7192-7200.
43. C. Chen, *Nature Reviews Chemistry*, 2018, **2**, 6-14.
44. M. C. Baier, M. A. Zuideveld and S. Mecking, *Angew. Chem., Int. Ed.*, 2014, **53**, 9722-9744.
45. A. Macchioni, *Chem. Rev.*, 2005, **105**, 2039-2074.
46. P. S. Kulyabin, G. P. Goryunov, M. I. Sharikov, V. V. Izmer, A. Vittoria, P. H. M. Budzelaar, V. Busico, A. Z. Voskoboynikov, C. Ehm, R. Cipullo and D. V. Uborsky, *J. Am. Chem. Soc.*, 2021, **143**, 7641-7647.
47. W. Kaminsky, *Journal of Polymer Science Part A: Polymer Chemistry*, 2004, **42**, 3911-3921.
48. P. Jutzi, C. Müller, A. Stammler and H.-G. Stammler, *Organometallics*, 2000, **19**, 1442-1444.

49. M. Brookhart, B. Grant and A. F. Volpe, Jr., *Organometallics*, 1992, **11**, 3920-3922.

50. L. K. Johnson, S. Mecking and M. Brookhart, *J. Am. Chem. Soc.*, 1996, **118**, 267-268.

51. L. Guo, S. Dai, X. Sui and C. Chen, *ACS Catal.*, 2016, **6**, 428-441.

52. W. Zhang, P. M. Waddell, M. A. Tiedemann, C. E. Padilla, J. Mei, L. Chen and B. P. Carrow, *J. Am. Chem. Soc.*, 2018, **140**, 8841-8850.

53. A. Ashuiev, M. Humbert, S. Norsic, J. Blahut, D. Gajan, K. Searles, D. Klose, A. Lesage, G. Pintacuda, J. Raynaud, V. Monteil, C. Copéret and G. Jeschke, *J. Am. Chem. Soc.*, 2021, **143**, 9791-9797.

54. M. P. McDaniel, M. D. Jensen, K. Jayaratne, K. S. Collins, E. A. Benham, N. D. Mcdaniel, P. K. Das, J. L. Martin, Q. Yang, M. G. Thorn and A. P. Masino, in *Tailor-Made Polymers*, eds. J. R. Severn and J. C. Chadwick, 2008, DOI: 10.1002/9783527621668.ch7, pp. 171-210.

55. S. Tsuji, D. C. Swenson and R. F. Jordan, *Organometallics*, 1999, **18**, 4758-4764.

56. D. B. Culver, R. W. Dorn, A. Venkatesh, J. Meeprasert, A. J. Rossini, E. A. Pidko, A. S. Lipton, G. R. Lief and M. P. Conley, *ACS Cent. Sci.*, 2021, **7**, 1225-1231.

57. D. B. Culver, J. Corieri, G. Lief and M. P. Conley, *Organometallics*, 2022, **41**, 892-899.

58. J. r. m. Joubert, F. ß. Delbecq, P. Sautet, E. L. Roux, M. Taoufik, C. Thieuleux, F. d. r. Blanc, C. Cop √ ©ret, J. Thivolle-Cazat and J.-M. Basset, *J. Am. Chem. Soc.*, 2006, **128**, 9157-9169.

59. A. Kermagoret, R. N. Kerber, M. P. Conley, E. Callens, P. Florian, D. Massiot, C. Coperet, F. Delbecq, X. Rozanska and P. Sautet, *Dalton Trans.*, 2013, **42**, 12681-12687.

60. S. Collins, W. M. Kelly and D. A. Holden, *Macromolecules*, 1992, **25**, 1780-1785.

61. I. M. Riddlestone, A. Kraft, J. Schaefer and I. Krossing, *Angew. Chem., Int. Ed.*, 2018, **57**, 13982-14024.

62. R. N. Kerber, A. Kermagoret, E. Callens, P. Florian, D. Massiot, A. Lesage, C. Copéret, F. ß. Delbecq, X. Rozanska and P. Sautet, *J. Am. Chem. Soc.*, 2012, **134**, 6767-6775.

63. A. Kermagoret, R. N. Kerber, M. P. Conley, E. Callens, P. Florian, D. Massiot, F. ß. Delbecq, X. Rozanska, C. Cop √ ©ret and P. Sautet, *J. Catal.*, 2014, **313**, 46-54.

64. J. Pelletier, J. Espinas, N. Vu, S. Norsic, A. Baudouin, L. Delevoye, J. Trébosc, E. Le Roux, C. Santini, J.-M. Basset, R. M. Gauvin and M. Taoufik, *Chem. Commun.*, 2011, **47**, 2979-2981.

65. K. C. Szeto, Z. R. Jones, N. Merle, C. Rios, A. Gallo, F. Le Quemener, L. Delevoye, R. M. Gauvin, S. L. Scott and M. Taoufik, *ACS Catal.*, 2018, **8**, 7566-7577.

66. S. D. Fleischman and S. L. Scott, *J. Am. Chem. Soc.*, 2011, **133**, 4847-4855.

67. Z. A. Taha, E. W. Deguns, S. Chattopadhyay and S. L. Scott, *Organometallics*, 2006, **25**, 1891-1899.

68. US Patent 5,643,847, 1995.

69. N. Millot, C. C. Santini, A. Baudouin and J.-M. Basset, *Chem. Commun.*, 2003, DOI: 10.1039/b304047j, 2034-2035.

70. D. W. Sauter, N. Popoff, M. A. Bashir, K. C. Szeto, R. M. Gauvin, L. Delevoye, M. Taoufik and C. Boisson, *Chem. Commun.*, 2016, **52**, 4776-4779.

71. Y.-J. Wanglee, J. Hu, R. E. White, M.-Y. Lee, S. M. Stewart, P. Perrotin and S. L. Scott, *J. Am. Chem. Soc.*, 2012, **134**, 355-366.

72. L. O. Müller, D. Himmel, J. Stauffer, G. Steinfeld, J. Slattery, G. Santiso-Quiñones, V. Brecht and I. Krossing, *Angew. Chem., Int. Ed.*, 2008, **47**, 7659-7663.

73. K. K. Samudrala, W. Huynh, R. W. Dorn, A. J. Rossini and M. P. Conley, *Angew. Chem., Int. Ed.*, 2022, **61**, e202205745.

74. H. Bohrer, N. Trapp, D. Himmel, M. Schleep and I. Krossing, *Dalton Trans.*, 2015, **44**, 7489-7499.

75. P. Erdmann, J. Leitner, J. Schwarz and L. Greb, *ChemPhysChem*, 2020, **21**, 987-994.

76. D. B. Culver, A. Venkatesh, W. Huynh, A. J. Rossini and M. P. Conley, *Chem. Sci.*, 2020, **11**, 1510 - 1517.

77. J. B. Miller, J. Schwartz and S. L. Bernasek, *J. Am. Chem. Soc.*, 1993, **115**, 8239-8247.

78. H. Großekappenberg, M. Reißmann, M. Schmidtmann and T. Müller, *Organometallics*, 2015, **34**, 4952-4958.

79. I. Del Rosal, I. C. Gerber, R. Poteau and L. Maron, *J. Phys. Chem. A*, 2010, **114**, 6322-6330.

80. R. J. Witzke, A. Chapovetsky, M. P. Conley, D. M. Kaphan and M. Delferro, *ACS Catal.*, 2020, DOI: 10.1021/acscatal.0c03350, 11822-11840.

81. M. Jezequel, V. r. Dufaud, M. J. Ruiz-Garcia, F. Carrillo-Hermosilla, U. Neugebauer, G. P. Niccolai, F. d. r. Lefebvre, F. ß. Bayard, J. Corker, S. Fiddy, J. Evans, J.-P. Broyer, J. Malinge and J.-M. Basset, *J. Am. Chem. Soc.*, 2001, **123**, 3520-3540.

82. L. A. Williams, N. Guo, A. Motta, M. Delferro, I. L. Fragal√†, J. T. Miller and T. J. Marks, *Proc. Nat. Acad. Sci. USA*, 2013, **110**, 413-418.

83. C. P. Nicholas, H. Ahn and T. J. Marks, *J. Am. Chem. Soc.*, 2003, **125**, 4325-4331.

84. M. Hino, S. Kobayashi and K. Arata, *J. Am. Chem. Soc.*, 1979, **101**, 6439-6441.

85. M. Hino and K. Arata, *Chem. Commun.*, 1980, DOI: 10.1039/c39800000851, 851-852.

86. D. Farcasiu, A. Ghenciu and J. Q. Li, *J. Catal.*, 1996, **158**, 116-127.

87. W. Chen, X. Yi, L. Huang, W. Liu, G. Li, D. Acharya, X. Sun and A. Zheng, *Cat. Sci. Tech.*, 2019, **9**, 5045-5057.

88. X. Li, K. Nagaoka, L. J. Simon, R. Olindo, J. A. Lercher, A. Hofmann and J. Sauer, *J. Am. Chem. Soc.*, 2005, **127**, 16159-16166.

89. J. E. Tabora and R. J. Davis, *J. Am. Chem. Soc.*, 1996, **118**, 12240-12241.

90. R. S. Drago and N. Kob, *J. Phys. Chem. B*, 1997, **101**, 3360-3364.

91. J. F. Haw, J. Zhang, K. Shimizu, T. N. Venkatraman, D.-P. Luigi, W. Song, D. H. Barich and J. B. Nicholas, *J. Am. Chem. Soc.*, 2000, **122**, 12561-12570.

92. R. C. Klet, D. M. Kaphan, C. Liu, C. Yang, A. J. Kropf, F. A. Perras, M. Pruski, A. S. Hock and M. Delferro, *J. Am. Chem. Soc.*, 2018, **140**, 6308-6316.

93. J. Rodriguez, D. B. Culver and M. P. Conley, *J. Am. Chem. Soc.*, 2019, **141**, 1484-1488.

94. A. M. Tatyana and I. K. Martin, *Russ. Chem. Rev.*, 1969, **38**, 795.

95. I. Kaljurand, A. Kütt, L. Soovӓli, T. Rodima, V. Mӓemets, I. Leito and I. A. Koppel, *J. Org. Chem.*, 2005, **70**, 1019-1028.

96. F. Haase and J. Sauer, *J. Am. Chem. Soc.*, 1998, **120**, 13503-13512.

97. I. Krossing and I. Raabe, *Angew. Chem., Int. Ed.*, 2004, **43**, 2066-2090.

98. S. P. Fisher, A. W. Tomich, S. O. Lovera, J. F. Kleinsasser, J. Guo, M. J. Asay, H. M. Nelson and V. Lavallo, *Chem. Rev.*, 2019, **119**, 8262-8290.

99. H. Yamamoto and K. Futatsugi, *Angew. Chem., Int. Ed.*, 2005, **44**, 1924-1942.

100. T. Xu, N. Kob, R. S. Drago, J. B. Nicholas and J. F. Haw, *J. Am. Chem. Soc.*, 1997, **119**, 12231-12239.

101. A. Kraft, J. Beck, G. Steinfeld, H. Scherer, D. Himmel and I. Krossing, *Organometallics*, 2012, **31**, 7485-7491.

102. W. R. Gunther, V. K. Michaelis, R. G. Griffin and Y. Román-Leshkov, *J. Phys. Chem. C*, 2016, **120**, 28533-28544.

103. J. P. Osegovic and R. S. Drago, *J. Phys. Chem. B*, 1999, **104**, 147-154.

104. P. Erdmann and L. Greb, *Angew. Chem., Int. Ed.*, 2022, **61**, e202114550.

105. X. Yi, Y.-K. Peng, W. Chen, Z. Liu and A. Zheng, *Acc. Chem. Res.*, 2021, **54**, 2421-2433.

106. W. Huynh and M. P. Conley, *Dalton Trans.*, 2020, **49**, 16453-16463.

107. C. A. Reed, *Acc. Chem. Res.*, 1998, **31**, 325-332.

108. H. F. T. Klare, L. Albers, L. Süsse, S. Keess, T. Müller and M. Oestreich, *Chem. Rev.*, 2021, **121**, 5889-5985.

109. C. A. Reed, Z. Xie, R. Bau and A. Benesi, *Science*, 1993, **262**, 402-404.

110. C. P. Gordon, C. Raynaud, R. A. Andersen, C. Copéret and O. Eisenstein, *Acc. Chem. Res.*, 2019, **52**, 2278-2289.

111. D. B. Culver, W. Huynh, H. Tafazolian, T.-C. Ong and M. P. Conley, *Angew. Chem., Int. Ed.*, 2018, **57**, 9520-9523.

112. G. Wu, D. Rovnyak, M. J. A. Johnson, N. C. Zanetti, D. G. Musaev, K. Morokuma, R. R. Schrock, R. G. Griffin and C. C. Cummins, *J. Am. Chem. Soc.*, 1996, **118**, 10654-10655.

113. K. B. Wiberg, J. D. Hammer, K. W. Zilm and J. R. Cheeseman, *J. Org. Chem.*, 1999, **64**, 6394-6400.

114. S. Berger, U. Fleischer, C. Geletneky and J. C. W. Lohrenz, *Chem. Ber.*, 1995, **128**, 1183-1186.

115. R. P. Young, C. R. Lewis, C. Yang, L. Wang, J. K. Harper and L. J. Mueller, *Magn. Reson. Chem.*, 2019, **57**, 211-223.

116. R. V. Viesser, L. C. Ducati, C. F. Tormena and J. Autschbach, *Chem. Sci.*, 2017, **8**, 6570-6576.

117. J. Sauer and R. Ahlrichs, *J. Chem. Phys.*, 1990, **93**, 2575-2583.

118. D. B. Culver and M. P. Conley, *Angew. Chem., Int. Ed.*, 2018, **57**, 14902-14905.

119. J. Bluemel, *J. Am. Chem. Soc.*, 1995, **117**, 2112-2113.

120. M. P. Conley, C. Copéret and C. Thieuleux, *ACS Catal.*, 2014, **4**, 1458-1469.

121. C. Zapilko, M. Widenmeyer, I. Nagl, F. Estler, R. Anwander, G. Raudaschl-Sieber, O. Groeger and G. Engelhardt, *J. Am. Chem. Soc.*, 2006, **128**, 16266-16276.

122. W. Song, D. M. Marcus, S. M. Abubakar, E. Jani and J. F. Haw, *J. Am. Chem. Soc.*, 2003, **125**, 13964-13965.

123. P. Preishuber-Pflugl and M. Brookhart, *Macromolecules*, 2002, **35**, 6074-6076.

124. A. Dorcier, N. Merle, M. Taoufik, F. Bayard, C. Lucas, A. de Mallmann and J. M. Basset, *Organometallics*, 2009, **28**, 2173-2178.

125. H. Tafazolian, D. B. Culver and M. P. Conley, *Organometallics*, 2017, **36**, 2385-2388.

126. M. Stalzer, M. Delferro and T. Marks, *Catal. Lett.*, 2015, **145**, 3-14.

127. J. Zhang, A. Motta, Y. Gao, M. M. Stalzer, M. Delferro, B. Liu, T. L. Lohr and T. J. Marks, *ACS Catal.*, 2018, **8**, 4893-4901.

128. J. Rodriguez and M. P. Conley, *Inorg. Chem.*, 2021, **60**, 6946-6949.

129. S. Dai, X. Sui and C. Chen, *Angew. Chem., Int. Ed.*, 2015, **54**, 9948-9953.

130. J. L. Rhinehart, L. A. Brown and B. K. Long, *J. Am. Chem. Soc.*, 2013, **135**, 16316-16319.

131. D. B. Culver, H. Tafazolian and M. P. Conley, *Organometallics*, 2018, **37**, 1001-1006.

132. P. Wucher, J. B. Schwaderer and S. Mecking, *ACS Catal.*, 2014, **4**, 2672-2679.

133. S. Dai and C. Chen, *Angew. Chem., Int. Ed.*, 2020, **59**, 14884-14890.

134. J. Gao, R. W. Dorn, G. P. Laurent, F. A. Perras, A. J. Rossini and M. P. Conley, *Angew. Chem., Int. Ed.*, 2022, **n/a**, e202117279.

135. J.-M. Basset, C. Coperet, D. Soulivong, M. Taoufik and J. T. Cazat, *Acc. Chem. Res.*, 2009, **43**, 323-334.

136. C. Copéret, D. P. Estes, K. Larmier and K. Searles, *Chem. Rev.*, 2016, **116**, 8463-8505.

137. S. L. Scott, A. Mills, C. Chao, J.-M. Basset, N. Millot and C. C. Santini, *J. Mol. Catal. A: Chem.*, 2003, **204,Äì205**, 457-463.

138. Y. S. Choi, E. G. Moschetta, J. T. Miller, M. Fasulo, M. J. McMurdo, R. M. Rioux and T. D. Tilley, *ACS Catal.*, 2011, **1**, 1166-1177.

139. M. Rimoldi, D. Fodor, J. A. van Bokhoven and A. Mezzetti, *Chem. Commun.*, 2013, **49**, 11314-11316.

140. S. Maier, S. P. Cronin, M.-A. Vu Dinh, Z. Li, M. Dyballa, M. Nowakowski, M. Bauer and D. P. Estes, *Organometallics*, 2021, **40**, 1751-1757.

141. D. Gajan, D. Levine, E. Zocher, C. Coperet, A. Lesage and L. Emsley, *Chem. Sci.*, 2011, **2**, 928-931.

142. H. Ahn, C. P. Nicholas and T. J. Marks, *Organometallics*, 2002, **21**, 1788-1806.

143. W. Gu, M. M. Stalzer, C. P. Nicholas, A. Bhattacharyya, A. Motta, J. R. Gallagher, G. Zhang, J. T. Miller, T. Kobayashi, M. Pruski, M. Delferro and T. J. Marks, *J. Am. Chem. Soc.*, 2015, **137**, 6770-6780.

144. P. G. Hayes, W. E. Piers and M. Parvez, *J. Am. Chem. Soc.*, 2003, **125**, 5622-5623.

145. S. J. Lancaster, O. B. Robinson, M. Bochmann, S. J. Coles and M. B. Hursthouse, *Organometallics*, 1995, **14**, 2456-2462.

146. D. J. Gillis, R. Quyoum, M.-J. Tudoret, Q. Wang, D. Jeremic, A. W. Roszak and M. C. Baird, *Organometallics*, 1996, **15**, 3600-3605.

147. S. M. Marie, N. C. P., B. Alak, M. Alessandro, D. Massimiliano and M. T. J., *Angew. Chem., Int. Ed.*, 2016, **55**, 5263-5267.

148. V. Dufaud and J.-M. Basset, *Angew. Chem., Int. Ed.*, 1998, **37**, 806-810.

149. U. Kanbur, G. Zang, A. L. Paterson, P. Chatterjee, R. A. Hackler, M. Delferro, I. I. Slowing, F. A. Perras, P. Sun and A. D. Sadow, *Chem*, 2021, **7**, 1347-1362.

150. M. E. O'Reilly, S. Dutta and A. S. Veige, *Chem. Rev.*, 2016, **116**, 8105-8145.

151. A. D. Sadow and T. D. Tilley, *Organometallics*, 2003, **22**, 3577-3585.

152. Z. Li, Q. Shi, X. Ma, Y. Li, K. Wen, L. Qin, H. Chen, W. Huang,

F. Zhang, Y. Lin, T. J. Marks and H. Huang, *Nature Communications*, 2022, **13**, 144.

153. J. Gao, L. Zhu and M. P. Conley, *J. Am. Chem. Soc.* 2023, *In Press*, DOI: 10.1021/jacs.2c13610.

154. M. Chabanas, V. Vidal, C. Copéret, J. Thivolle-Cazat and J.-M. Basset, *Angew. Chem., Int. Ed.*, 2000, **39**, 1962-1965.

155. W. H. Bernskoetter, C. K. Schauer, K. I. Goldberg and M. Brookhart, *Science*, 2009, **326**, 553-556.

156. H. M. Yau, A. I. McKay, H. Hesse, R. Xu, M. He, C. E. Holt and G. E. Ball, *J. Am. Chem. Soc.*, 2016, **138**, 281-288.

157. J. D. Watson, L. D. Field and G. E. Ball, *J. Am. Chem. Soc.*, 2022, **144**, 17622-17629.

158. S. A. Bartlett, N. A. Besley, A. J. Dent, S. Diaz-Moreno, J. Evans, M. L. Hamilton, M. W. D. Hanson-Heine, R. Horvath, V. Manici, X.-Z. Sun, M. Towrie, L. Wu, X. Zhang and M. W. George, *J. Am. Chem. Soc.*, 2019, **141**, 11471-11480.

159. J. A. Calladine, S. B. Duckett, M. W. George, S. L. Matthews, R. N. Perutz, O. Torres and K. Q. Vuong, *J. Am. Chem. Soc.*, 2011, **133**, 2303-2310.

160. K. A. Reid and D. C. Powers, *Chem. Commun.*, 2021, **57**, 4993-5003.

161. A. J. Martínez-Martínez, B. E. Tegner, A. I. McKay, A. J. Bukvic, N. H. Rees, G. J. Tizzard, S. J. Coles, M. R. Warren, S. A. Macgregor and A. S. Weller, *J. Am. Chem. Soc.*, 2018, **140**, 14958-14970.

162. T. M. Boyd, B. E. Tegner, G. J. Tizzard, A. J. Martínez-Martínez, S. E. Neale, M. A. Hayward, S. J. Coles, S. A. Macgregor and A. S. Weller, *Angew. Chem., Int. Ed.*, 2020, **59**, 6177-6181.

163. A. I. McKay, A. J. Bukvic, B. E. Tegner, A. L. Burnage, A. J. Martínez-Martínez, N. H. Rees, S. A. Macgregor and A. S. Weller, *J. Am. Chem. Soc.*, 2019, **141**, 11700-11712.

164. A. J. Bukvic, A. L. Burnage, G. J. Tizzard, A. J. Martínez-Martínez, A. I. McKay, N. H. Rees, B. E. Tegner, T. Krämer, H. Fish, M. R. Warren, S. J. Coles, S. A. Macgregor and A. S. Weller, *J. Am. Chem. Soc.*, 2021, **143**, 5106-5120.

165. L. R. Doyle, M. R. Galpin, S. K. Furfari, B. E. Tegner, A. J. Martínez-Martínez, A. C. Whitwood, S. A. Hicks, G. C. Lloyd-Jones, S. A. Macgregor and A. S. Weller, *Organometallics*, 2022, **41**, 284-292.

166. C. G. Royle, L. Sotorrios, M. R. Gyton, C. N. Brodie, A. L. Burnage, S. K. Furfari, A. Marini, M. R. Warren, S. A. Macgregor and A. S. Weller, *Organometallics*, 2022, **41**, 3270-3280.

167. D. M. Kaphan, R. C. Klet, F. A. Perras, M. Pruski, C. Yang, A. J. Kropf and M. Delferro, *ACS Catal.*, 2018, **8**, 5363-5373.

168. C. P. Gordon, D. B. Culver, M. P. Conley, O. Eisenstein, R. A. Andersen and C. Copéret, *J. Am. Chem. Soc.*, 2019, **141**, 648-656.

169. D. Lapointe and K. Fagnou, *Chem. Lett.*, 2010, **39**, 1118-1126.

170. Z. H. Syed, D. M. Kaphan, F. A. Perras, M. Pruski, M. S. Ferrandon, E. C. Wegener, G. Celik, J. Wen, C. Liu, F. Dogan, K. I. Goldberg and M. Delferro, *J. Am. Chem. Soc.*, 2019, **141**, 6325-6337.

171. J. Choi, A. H. R. MacArthur, M. Brookhart and A. S. Goldman, *Chem. Rev.*, 2011, **111**, 1761-1779.

172. M. O. Akram, J. R. Tidwell, J. L. Dutton and C. D. Martin, *Angew. Chem., Int. Ed.*, 2022, **61**, e202212073.

173. J. Rodriguez and M. P. Conley, *Org. Lett.*, 2022, **24**, 4680-4683.

174. A. Chapovetsky, R. M. Kennedy, R. Witzke, E. C. Wegener, F. Dogan, P. Patel, M. Ferrandon, J. Niklas, O. G. Poluektov, N. Rui, S. D. Senanayake, J. A. Rodriguez, N. J. Zaluzec, L. Yu, J. Wen, C. Johnson, C. J. Jenks, A. J. Kropf, C. Liu, M. Delferro and D. M. Kaphan, *ACS Catal.*, 2022, **12**, 7233-7242.